Advanced Field Interpolation from Plane-Polar Samples: Experimental Verification

O. M. Bucci, *Fellow, IEEE*, G. D'Elia, and M. D. Migliore

***Abstract*— A new and advanced sampling technique far-field interpolation with a nonredundant number of samples on plane-polar geometry has been experimentally validated for cases of both complex and only-amplitude measurements. Experimental results show good stability of the interpolation algorithm with respect to noise and the lack of samples in the case of a limited scanning area.**

***Index Terms*—Measurement, sampling methods.**

I. Introduction

THE problem of an efficient (i.e., accurate and computationally effective) representation of radiated or scattered fields is of great relevance in electromagnetics. As compared with those based on modal or asymptotic expansions, sampling representations are very attractive since the expansion coefficients are the field values at the sampling points, i.e., the available measured (or computed) quantities and the basis functions are simple and universal. Following the introduction of the concept of field effective bandwidth [1], more and more efficient sampling field representations over canonical scanning surfaces have been developed [2]–[4].

Recently the sampling approach has been extended also to the bi-polar system and has been experimentally validated for this geometry [5], [6]. Based on the concept of effective bandwidth, the concept of the field's number of degrees of freedom has also been rigorously introduced [7].

However, a theoretically relevant inconsistency of the above mentioned formulas is related to the number of required samples, which is finite for a closed bounded surface and, in principle, infinite for an unbounded one. On the contrary, on the basis of the concept of the field's number of degrees of freedom, we can say that an effective and nonredundant sampling series should require the same number of samples, regardless of the observation surface. Furthermore, this number should depend not only on the *size* but also on the *shape* of the source, whereas in the available sampling representations only the size of the source is taken into account, thus leading to a further redundancy in the case of nonspherical sources.

Very recently, new and advanced sampling representations have been introduced [8]–[10] that overcome these drawbacks. They are based on a generalization of the approach followed in [1] and exploit a nonredundant number of samples related to the dimensions and geometry of the source. This feature allows a decrease in the required number of samples in many significant cases such as for planar sources. The aim of this paper is to present an experimental verification of these new results for a plane-polar scanning geometry and a planar source. A brief description of the recently introduced sampling series is given in Section II. The measurement facility is described in Section III-A and the experimental results are reported in Section III-B. In order to check the overall performance of the experimental setup, an ideal simulated example is also elaborated in the final section.

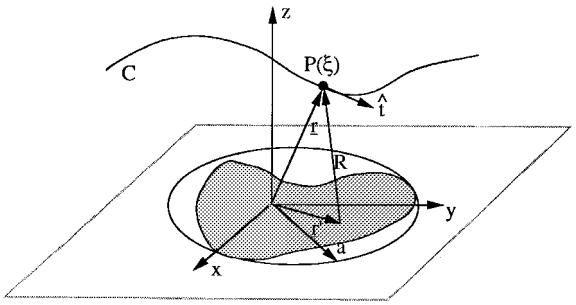

Fig. 1. Geometry of the problem.

II. The Optimal Sampling Algorithm

A brief summary of the theory of advanced sampling interpolation (developed in [8]–[10]) is reported in this section by referring to a planar source and a plane-polar scanning.

Let us consider a planar source S contained in a circle of radius a (Fig. 1) and let us define the "reduced" field

$$\underline{F}(\xi) = \exp[j\gamma(\xi)]\underline{E}(\xi) \tag{1}$$

where $\underline{E}(\xi)$ is the radiated field observed along the curve C, $\xi = \xi(s)$ is the curve parameterization, s being the arc length, and $\gamma(\xi)$ is a phase function to be determined. Provided that $\gamma(\xi)$ and the chosen parameterization do not introduce spurious singularities, the reduced field is a function analytic in ξ. Then, following [1], it can be shown hat $\underline{F}$ can be approximated by means of a function bandlimited to w (say

Manuscript received July 28, 1995; revised September 26, 1997.

The authors are with the Dipartimento di Ingegneria Elettronica, Universita' di Napoli, Napoli, 80125 Italy.

Publisher Item Identifier S 0018-926X(98)01488-4.

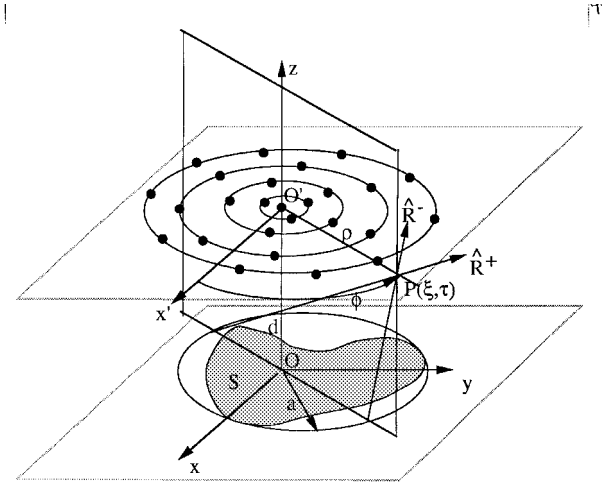

Fig. 2. Plane-polar scanning geometry.

$\underline{F}_w$) where $w = \chi_1 W$, χ_1 is a factor greater than one and

$$W = \max_{\xi} \left[\max_{\underline{r}'} |\partial(\gamma(\xi) - \beta R(\underline{r}', \xi))/\partial\xi| \right] = \max_{\xi} w_0(\xi) \tag{2}$$

with $R(\underline{r}', \xi) = |\underline{r}(\xi) - \underline{r}'|$ (Fig. 1). The excess bandwidth factor χ_1 makes it possible to control the approximation error, which has a step-like behavior and decreases exponentially with $W(\chi_1 - 1)^{3/2}$. In the case of electrically large antennas ($\beta a \gg 1$), this error becomes negligible for a value of χ_1 slightly larger than one so that W is naturally identified with the effective field bandwidth corresponding to the chosen parameterization and phase factor.

In order to reduce the bandwidth, it is convenient to minimize, for each value of ξ the term $w_0(\xi)$ in (2), i.e., to set $d\gamma/d\xi$ equal to the mean between the maximum and minimum value assumed by $\beta\, dR(\underline{r}', \xi)/d\xi$ when $\underline{r}'$ varies in the circle containing the source. This choice leads to the phase factor γ and, thus, to W as well as to the the sampling rate (with respect to the variable ξ) corresponding to $w = \chi_1 W$.

However, it must be noted that for the values of ξ such that $w_0(\xi) < W$ an oversampling does occur (i.e., a number of samples larger than the minimum possible one is exploited in the neighborhood of that value of ξ). In order to eliminate this redundancy, the parameterization $\xi(s)$ must be chosen in such a way that, for instance, $w_0(\xi) = \text{const} = W = \beta a$.

For a radial line in a plane-polar scanning geometry one obtain [8]–[10] (see Fig. 2)

$$\xi = (R^+ - R^-)/2a; \quad \gamma(\xi) = \beta(R^+ + R^-)/2 \tag{3}$$

while for an azimuthal circumference the optimal parameterizaton (say τ) is given by

$$\tau = \phi(R^+ - R^-)/2a \tag{4}$$

In the latter case, the phase function γ is constant and, therefore, unessential.

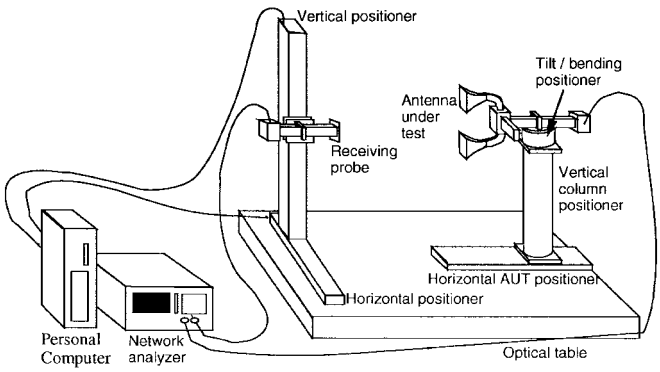

Fig. 3. Experimental setup.

TABLE I
EXPERIMENTAL SETUP DESCRIPTION

Vertical positioner and motor: Physik Instrumente M-900.455 and M427.20
Horizontal positioner and motor: Physik Instrumente M- 900.454 and M427.20
Horizontal AUT positioner: optical bench Ealing 36-0073
Tilt/Bending positioner: Melles Griot 07TTA502
Personal computer: 80486 processor based
Network Analyzer: HP 8719
Receiving probe: flanged waveguide WR62
Antenna under test : two horns Narda DBF 639
Magic T: Narda DBF 650
Absorbers: pyramidal absorbers Plessy AFP12 (not shown in the figure)

It should be noted that since the reduced field is sampled uniformly with respect to ξ, a nonuniform sampling with respect to the radial coordinate ρ is obtained. In particular, we have a finite number of samples $N \cong 2\beta a/\pi$ when the observation point moves along a radial line from $-\infty$ to $+\infty (-1 \le \xi \le 1)$. Analogously, on an azimuthal circumference the number of samples is $N \cong \beta(R^+ - R^-)$ so that the total number of samples on the whole (unbounded) observation plane is finite and is given by $N \cong (\beta a)^2/\pi$. As anticipated in the Introduction, the number of samples required by the new sampling approach (which is essentially equal to the number of degrees of freedom of the field radiated by a planar source) is finite even if the observation surface is unbounded and equal to about *one half* of the degrees of freedom of a spherical source having the same radius [4].

Based on the above results, a complete interpolation algorithm can be obtained for a plane-polar scanning geometry by applying either the canonical cardinal series (CS) [1] or the central interpolation (CI) series [3], [8], [10] to the reduced field F_w. In the CI scheme a slight oversampling of the field is required in order to make negligible the truncation error for a given number of retained samples [3]. In the following, the corresponding oversampling factor will be called χ_2. The general form of the interpolation series for both schemes is

$$\underline{E}(\xi, \phi) = e^{-j\gamma(\xi)} \sum_n e^{j\gamma(n\Delta\xi)} \sum_m [\underline{E}(n\Delta\xi, m\Delta\phi_n)\Theta_n (\phi - m\Delta\phi)]\Omega(\xi - n\Delta\xi) \tag{5}$$

wherein the explicit expressions of the radial and angular sampling intervals as well as the expressions of the

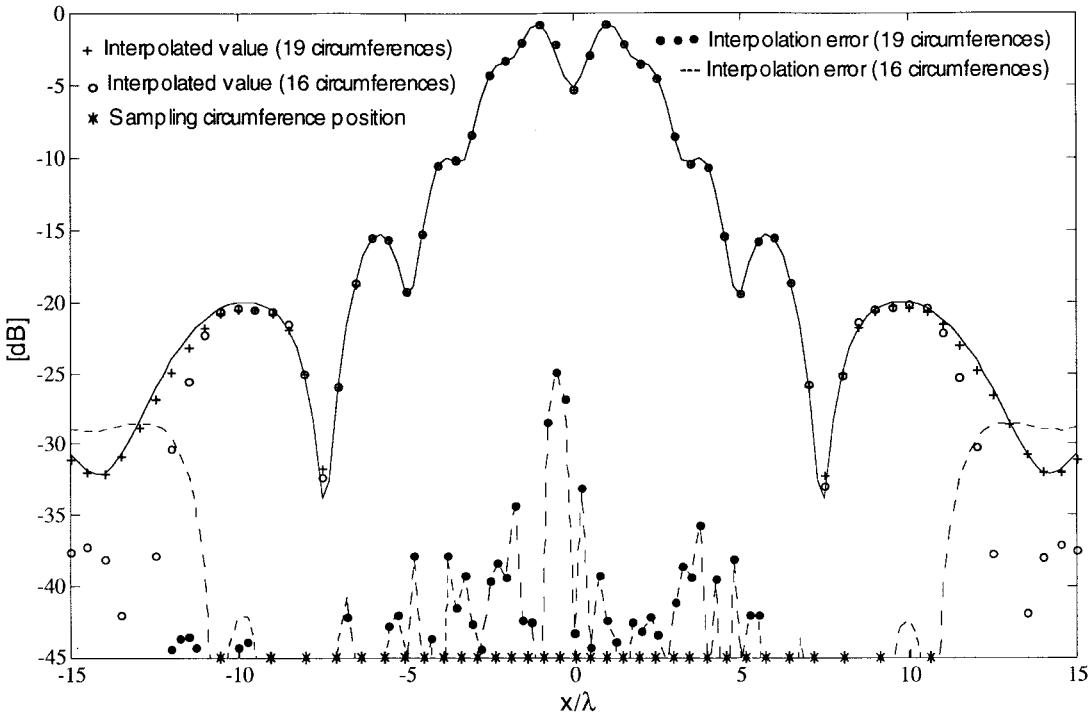

Fig. 4. Numerical simulation—comparison between intepolated and computed fields: $\chi_1 = 1.2$, $\chi_2 = 1.15$, $p = q = 5$.

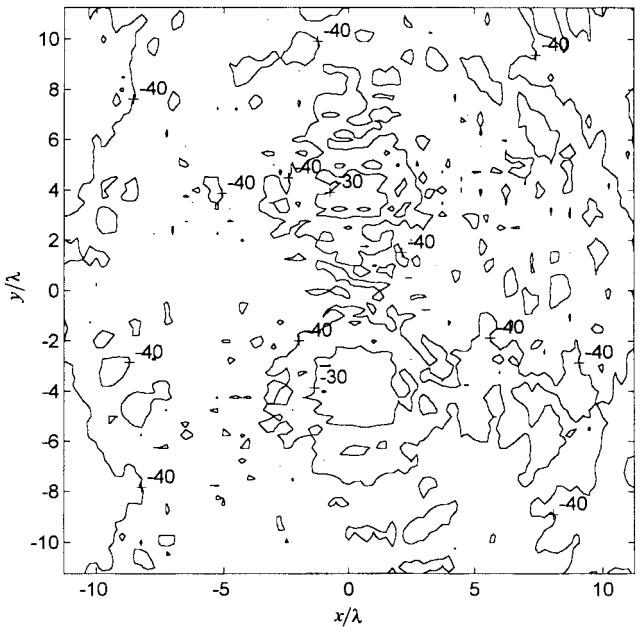

Fig. 5. CS interpolation ($\chi_1 = 1.2$). Normalized interpolation error (decibels) contour plot.

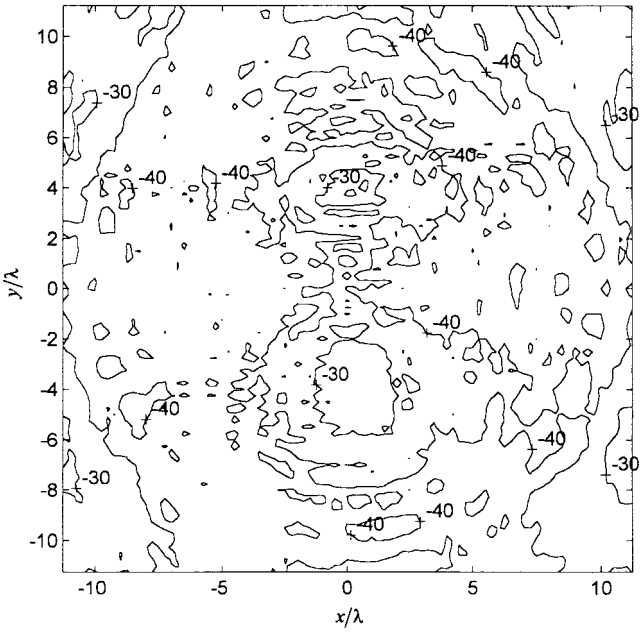

Fig. 6. CI interpolation ($\chi_1 = 1.2$, $\chi_2 = 1.15$, $p = q = 5$). Normalized interpolation error (decibels) contour plot.

interpolating functons Θ_n and Ω are reported in [10, Tables (1), (2)].

While in the CS scheme, the index n and m are extended to all relevant samples along the mth radial line and the nth circumference, respectively, in the CI scheme n and m are extended only to a small number of samples along ξ and ϕ, say $2p$ and $2q$ respectively, centered on the observation point. Accordingly, the central interpolation scheme is numerically more efficient than the CS scheme. Furthermore, it avoids the influence of the measurement errors made in the high-level field regions on the reconstruction of the field in the low-level field region.

The above results can also be applied to the squared amplitude of the radiated field which is, obviously, a quasi-bandlimited function with a bandwidth twice that of the "reduced" field.

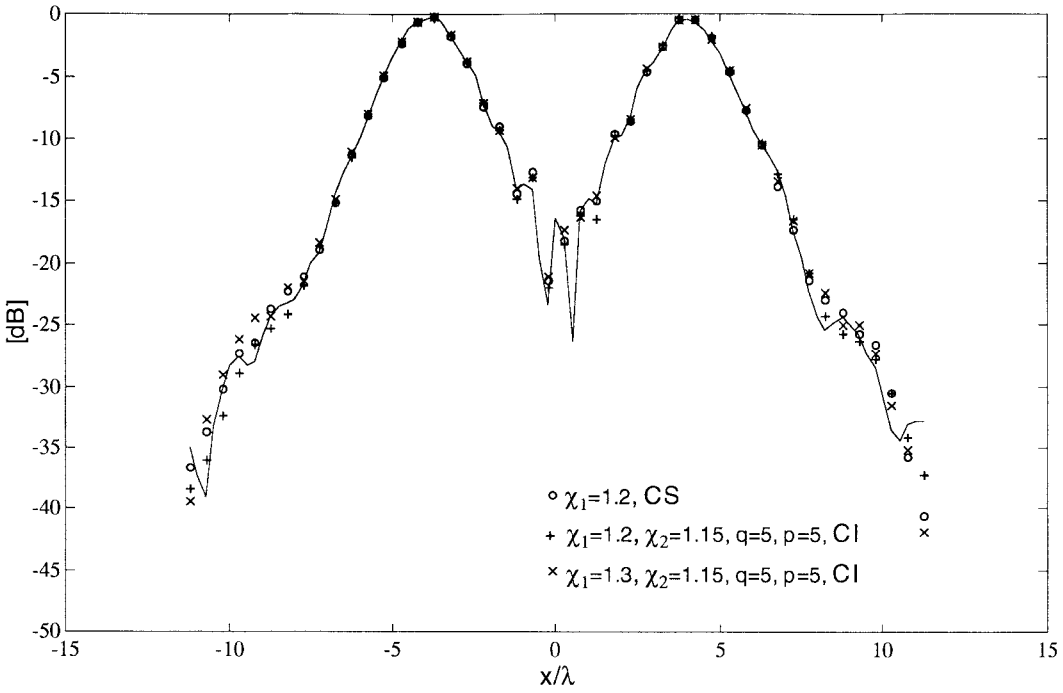

Fig. 7. Amplitude of the reference (continuous line) and interpolated signal along the line $x = 0$.

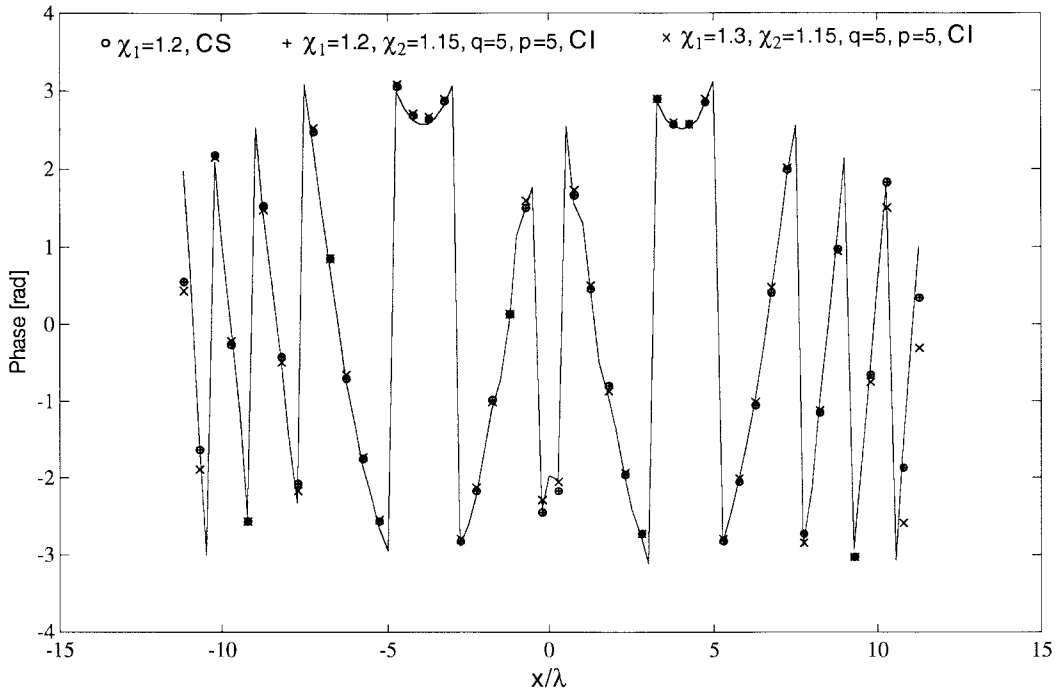

Fig. 8. Phase of the reference (continuous line) and interpolated signal (degrees) along the line $x = 0$.

III. Experimental Validation

The considerations made in the previous section refer to the field radiated by the source. However, in any experimental setup, the measured quantity is the voltage received by the probe so that prior to validate the sampling approach it must be shown that the measured voltage, over the observation surface, *also* has an effective bandwidth equal to that of the radiated field. To this end, let us recall that the voltage received at a given observation point over the scanning plane by any (nonrotating) probe can be expressed as a linear superposition of the spatial derivatives of the radiated field at the same point with coefficients depending only on the spherical expansion coefficients of the field radiated by the probe [11]. Now, by paralleling the development followed for the radiated field, each field spatial derivative of not too high an order can be

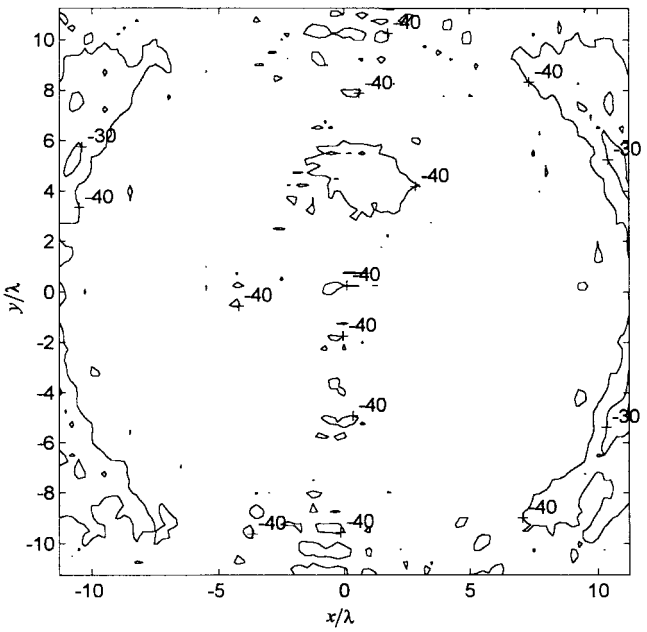

Fig. 9. CS amplitude interpolation ($\chi_1 = 1.2$). Normalized interpolation error (decibels) contour plot.

approximated by means of a bandlimited function with the same bandwidth as the field (a similar asymptotic evaluation of the bandlimitation error is possible and a similar step-like behavior of such error results). Accordingly, provided that there are only a limited number of relevant probe spherical harmonics (as happen for any properly designed probe), a linear combination of such derivatives and, hence, the measured voltage also admits the same equivalent bandwidth. In conclusion, it can be stated that the sampling series considered in the previous section applies to the complex as well as to the square amplitude of the measured probe voltage.

A. Experimental Setup

The interpolation algorithm described in the preceding section has been experimentally validated using a low-cost and flexible near-field measurement system developed at the Microwave Laboratory of the Electronics Department of the University of Napoli, "Federico II," Italy. The measurement setup is schematically shown in Fig. 3.

The antenna under test (AUT) is held by a Tilt/Rotation platform that makes it possible to position the AUT parallel to the scanning plane, while the Z-axis position is set by means of an optical bench. The receiving probe is connected with a customized probe holder to a 600-mm-long vertical linear positioner mounted on a 600-mm-long horizontal linear positioner, both having computer controlled dc motors. The receiving probe and the AUT positioning system are mounted on a 1.2 m $\times$ 1.8 m optical table. Pyramidal absorbers are positioned in order to minimize reflections and to obtain a sufficiently "quiet" measurement zone.

The radio frequency (RF) section is based on a vector network analyzer connected to a personal computer via IEEE488. GoreTex flexible cables were used to connect the receiving probe to the receiver, while a semiflexible cable RG402 was adopted to feed the AUT.

The scanning system operates under the control of a program running on a personal computer with a GP-IB II and a dc motor control card. The program makes it possible to select various parameters such as the working frequency (up to 13 GHz), the microwave generator output power, the number of acquisitions on the plane, the kind of sampling grid (the maximum scanning area is 600 mm $\times$ 600 mm large) and the corresponding parameters.

More details on the experimental setup are collected in Table I.

B. Experimental Results

Prior to performing experimental tests, a numerical simulation was performed in order to estimate the "best" results to be expected in an ideal case. It must be noted that the main problem encountered when exploiting the interpolation series of the previous section is related to the truncation of the measurement zone, i.e., to the fact that even if the number of circumferences on which the field must be sampled is finite, their radius increases rapidly so that the last circumferences usually fall outside the scanning area. In order to investigate this situation, we simulated the experimental conditions described in the following by considering an array of $\lambda/2$ spaced 13 $\times$ 23 dipoles enclosed by a circumference of radius 6.9 λ and an observation plane 5.8 λ far from the source. The numerically computed near-field amplitude on the $y = 0$ line $(-15\lambda < x < 15\lambda)$ of such plane is shown as a continuous line in Fig. 4.

The interpolated field has been evaluated using a CI algorithm with $\chi_1 = 1.2$, $\chi_2 = 1.15$, and $p = q = 5$. The results obtained by exploiting the inner 16 and all the 19 circumferences covering the whole plane are shown by circles and crosses, respectively. The corresponding interpolation error is shown as a dashed and dotted line, respectively. The asterisk on the bottom of the figure shows the radial positions of the inner 16 circumferences. As can be seen, notwithstanding the lack of external samples, the error inside the 16th circumference is quite low—between -25 and -40 dB. Note also that the behavior of the error follows that of the field, i.e., the *relative* error is essentially constant.

Let us now consider the experimental results.

The measurements were performed at 13 GHz using two horns (see Fig. 3) working on P-band (12.4–18 GHz). The two horns were fed in phase and constituted a linearly polarized planar source contained in a circle of radius $a = 6.92\lambda$. The scanning plane was placed at a distance $d = 5.77\lambda$ from the aperture plane of the antenna under test. An open flanged WR-62 waveguide was adopted as the probe.

As preliminary step, the radiated field was measured on a rectangular regular grid of 91 $\times$ 91 $\lambda/4$ spaced points in order to get a reference distribution to be compared with the results obtained by the application of the plane-polar interpolation algorithms.

Plane-polar scanning measurements were then performed for different values of χ_1 and χ_2. First, we set $\chi_1 = 1.2$ and $\chi_2 = 1$. Due to the finite dimension of the scanning

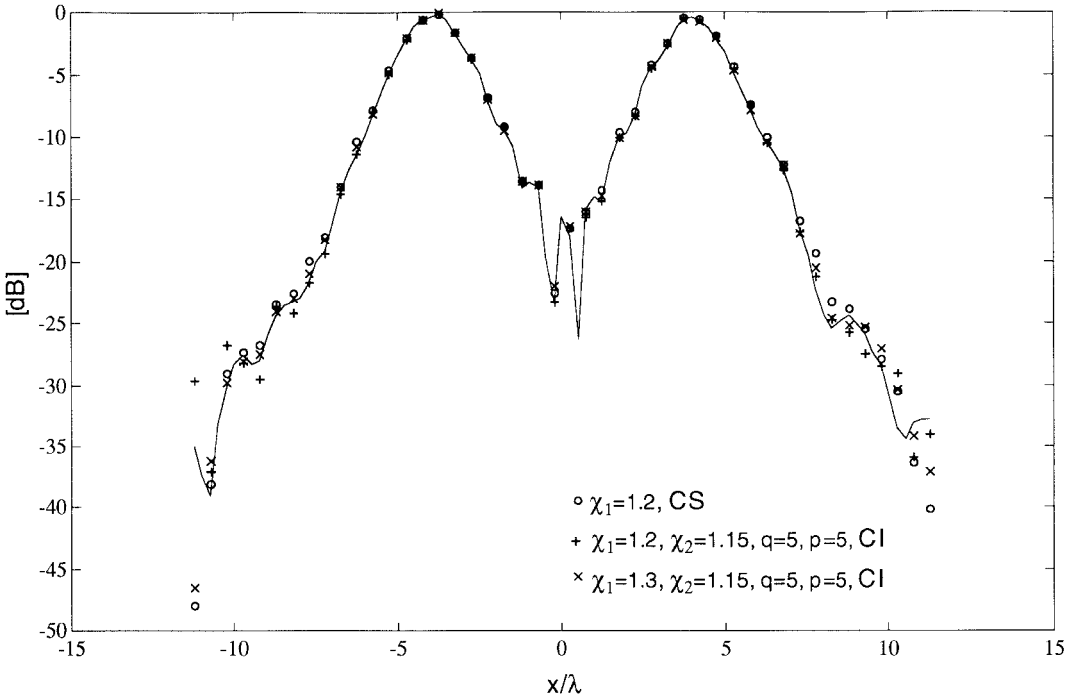

Fig. 10. Amplitude of the reference (continuous line) and interpolated (from only amplitude samples) signal along the line $x = 0$.

TABLE II
INTERPOLATED DATA (C: COMPLEX SAMPLES, SA: SQUARE AMPLITUDE SAMPLES)

		Optimal sampling							**$\lambda/2$ spacing**	**standard**
Fig	Data	χ_1	χ_2	p,q	N° Circumferences		N° samples		**rectangular sampling**	**plane-polar sampling**
					Meas..	whole plane	Meas.	whole plane	N° samples	N° samples
5, 7, 8	C	1.2	-	-	14	16	725	923	1849	1442
-	C	1.3	-	-	15	17	842	1054	1764	1518
6, 7, 8	C	1.2	1.15	5	16	19	927	1272	1849	1654
7, 8	C	1.3	1.15	5	17	20	1070	1435	1681	1717
9,10	SA	1.2	-	-	28	33	2741	3726	7396	5618
-	SA	1.3	-	-	30	35	3229	4282	7056	6210
10	SA	1.2	1.15	5	32	38	3577	4931	7225	6462
10	SA	1.3	1.15	5	35	41	4374	5846	7569	7140

area, only 14 circumferences (corresponding to 725 samples) fell inside the scanning area instead of the 16 circumferences covering the whole plane (corresponding to 923 samples). The normalized amplitude of the interpolation error, i.e., of the difference between the (complex) signal interpolated by means of the CS series and the measured "reference" one normalized to the maximum value of the reference amplitude is shown in Fig. 5.

Then a second set of measurements corresponding to $\chi_1 = 1.2$, $\chi_2 = 1.15$ was performed. The amplitude of the normalized interpolation error obtained by exploiting the CI scheme with $p = q = 5$ is shown in Fig. 6. In this case 16 circumferences (927 samples) are included in the measurement zone out of the 19 (1272 samples) lying in the whole measurement plane.

A comparison between the amplitude of the reference signal (solid line) and the results obtained from both the CS (circles) and the CI (crosses) interpolation scheme on the cut line $x = 0$ is shown in Fig. 7. Excluding the peripheral region wherein the high relative error is caused mainly by the lack of the outer circumferences, the CI interpolation is, in general, more precise than the CS due to the presence of the sampling window functions, which keep down the truncation error.

In Fig. 8 the same comparison is made by referring to the phase of the field on the line $x = 0$.

The results obtained by assuming a slightly higher bandwidth enlargement factor $(\chi_1 = 1.3)$ are shown in these figures with the label "x" and are almost the same than the previous ones. They show that the bandlimitation error corresponding

to an enlargement factor $\chi_1 = 1.2$ is sufficiently low. The use of a large bandwidth does not substantially improve the interpolation; on the contrary, due to the larger bandwidth, the associated noise is higher so that the interpolation error is slightly increased.

An experimental check has also been performed in the case of a direct interpolation of the squared amplitude. The normalized interpolation error obtained from the CS series $(\chi_1 = 1.2)$ is shown in Fig. 9. In this case, 28 out of 33 circumferences fell into the scanning plane.

Similar results are obtained from the CI algorithm by assuming $\chi_1 = 1.2$, $\chi_2 = 1.15$, $p = 5$, $q = 5$, and retaining 32 of the overall 38 circunferences.

The results obtained by exploiting the CS and CI algorithm on the line $x = 0$ are reported in Fig. 10 (circles and crosses, respectively) together with the reference field (solid line). Due to the higher number of circumferences inside the scanning area, the field interpolation is very satisfactory up to -20 dB level, with a normalized error lower than in the previous cases.

In the same figure, the results obtained by applying the CI with $\chi_1 = 1.3$, $\chi_2 = 1.15$, $p = 5$, $q = 5$, and retaining 35 of the overall 41 circunferences are also reported (with the symbol "x").

A summary of the acquired data is reported in Table II, wherein the number of samples required by the standard $\lambda/2$ rectangular and plane polar (with a $\lambda/2$ radial spacing) sampling are also reported. Of course, the same values of χ_1 and χ_2 have been considered and only the samples falling in the measurement region have been taken into account. It is worth noting that the ratio between the number of samples of the standard sampling series with respect to the optimal one dramatically increases with the size of the measurement region. When the measurement region includes all the circles of the optimal sampling with $\chi_1 = 1.2$, $\chi_2 = 1.15$, this ratio becomes 37 and nine for the standard plane-rectangular and plane-polar sampling, respectively.

In conclusion, we can state that the plane-polar interpolation series considered in Section II have been experimentally validated with reference to both the radiated field and its square amplitude. In particular, the above results show that the nonredundant data (which are significantly less than those exploited in the standard approaches) makes it possible to obtain a satisfactory interpolation of the field even if, due to the very limited scanning area (a circle with a radius equal to 11λ for a source with a radius $a \cong 7\lambda$ in the worked example), the outermost sample points cannot be measured. Furthermore, as expected, the errors obtained using the CI algorithm are slightly lower than the ones obtained by the CS algorithm.

ACKNOWLEDGMENT

The authors would like to thank A. De Gregorio for his contribution in performing the near-field measurements.

REFERENCES

[1] O. M. Bucci and G. Franceschetti, "On the spatial bandwidth of scattered fields," *IEEE Trans. Antennas Propagat.*, vol. AP-35, pp. 1445–1455, Dec. 1987.

[2] O. M. Bucci and C. Gennarelli, "Use of sampling expansions in near-field far-field transformations: The cylindrical case," *IEEE Trans. Antennas Propagat.*, vol. 36, pp. 830–835, June 1988.

[3] O. M. Bucci, C. Gennarelli, and C. Savarese, "Fast and accurate near-field far-field transformation by sampling interpolation of plane-polar measurements," *IEEE Trans. Antennas Propagat.*, vol. 39, pp. 48–55, Jan. 1991.

[4] ——, "Optimal interpolation of radiated fields over a sphere," *IEEE Trans. Antennas Propagat.*, vol. 39, pp. 1633–1643, Nov. 1991.

[5] L. I. Williams, Y. Rahmat-Samii, and R. G. Yaccarino, "The bi-polar planar near-field measurement technique—Part I: Implementation and measurement comparison," *IEEE Trans. Antennas Propagat.*, vol. 42, pp. 184–195, Feb. 1994.

[6] R. G. Yaccarino, Y. Rahmat-Samii, and L. I. Williams, "The bi-polar planar near-field measurement technique—Part II: Near-field to far-field transformation and holographic imaging methods," *IEEE Trans. Antennas Propagat.*, vol. 42, pp. 196–204, Feb. 1994.

[7] O. M. Bucci and G. Franceschetti, "On the degrees of freedom of scattered fields," *IEEE Trans. Antennas Propagat.*, vol. 37, pp. 918–926, July 1989.

[8] O. M. Bucci, C. Gennarelli, G. Riccio, and C. Savarese, "Precise interpolation of electromagnetic fields over a cylinder from a nonredundant, finite number of samples," in *Proc. PIERS 1994 Int. Symp.*, Noordwijk, The Netherlands, July 1994, p. 316.

[9] ——, "Efficient interpolation of electromagnetic fields over a plane from a non redundant, finite number of samples," in *Proc. X RinEM*, Cesena, Italy, Sept. 1994, pp. 339–342.

[10] O. M. Bucci and G. D'Elia, "Advanced sampling techniques in electromagnetics," *Rev. Radio Sci.*, pp. 177–204, 1993–1996.

[11] A. D. Yaghjian R. C. Wittman, "The receiving antenna as a linear differential operator: Application to spherical near-field scanning," *IEEE Trans. Antennas Propagat.*, vol. AP-33, pp. 1175–1185, Nov. 1985.

O. M. Bucci (SM'82–F'93), for photograph and biography, see p. 994 of the June 1997 issue of this TRANSACTIONS.

G. D'Elia, for photograph and biography, see p. 1225 of the November 1995 issue of this TRANSACTIONS.

M. D. Migliore, for photograph and biography, see p. 994 of the June 1997 issue of this TRANSACTIONS.